

Neutrino Factory/Muon Collider Front End Study 2A-like Simulation Cross Check and Economization of RF Cavities

Cary Y. Yoshikawa^{a,b} and David V. Neuffer^a

^a*Fermilab, Batavia, IL, USA*

^b*Muons, Inc., Batavia, IL, USA*

Abstract. Earlier studies on the front end of a neutrino factory or muon collider have relied on a single simulation tool, ICOOL. We present here a cross-check against another simulation tool, G4beamline. We also perform a preliminary study in economizing the number of RF cavity frequencies and gradients. We conclude with a discussion of future studies.

Keywords: neutrino factory, muon collider, front end, muon cooling, muon capture

PACS: Replace this text with PACS numbers; choose from this list: <http://www.aip.org/pacs/index.html>

INTRODUCTION

One of the major challenges in realizing a neutrino factory or muon collider is establishing a front end that captures and cools a sufficiently high number of muons that feed the downstream accelerating structures. The current baseline study 2A (or 2B) [1] for a neutrino factory or muon collider relied on ICOOL [2] for much of its design. A cross check is presented here utilizing G4beamline (G4BL) [3], which is based on GEANT4 [4]. Beyond the consistency verification, a preliminary study is performed on economizing the number of RF cavity frequencies and gradients. We conclude with a discussion of future studies.

CONSISTENCY VERIFICATION BETWEEN ICOOL AND G4BEAMLIN

The layout of the front end that is studied is a snapshot of an evolving design based on Study 2A [1] and is shown in FIGURE 1, along with some parameters listed in TABLE 1. Common to the ICOOL and G4beamline simulations that are being compared were the input events generated by MARS [5] that simulated what is expected out of a MERIT-like target system [6], where in this case protons of 8 GeV (kinetic energy) impinge on a jet stream of mercury. Both protons and Hg jet are at angles relative to the nominal z-axis that defines the geometry of the front end.

Snapshots in momentum vs. time for the evolution of pions and muons from start of the capture (tapered) solenoid to end of cooler are shown in FIGURE 2 through FIGURE 8. Before quantifying the phase space at these locations, it is readily seen that there are differences between ICOOL and G4beamline in the cooling sections. Causes for these differences and remedies are discussed in the following subsection.

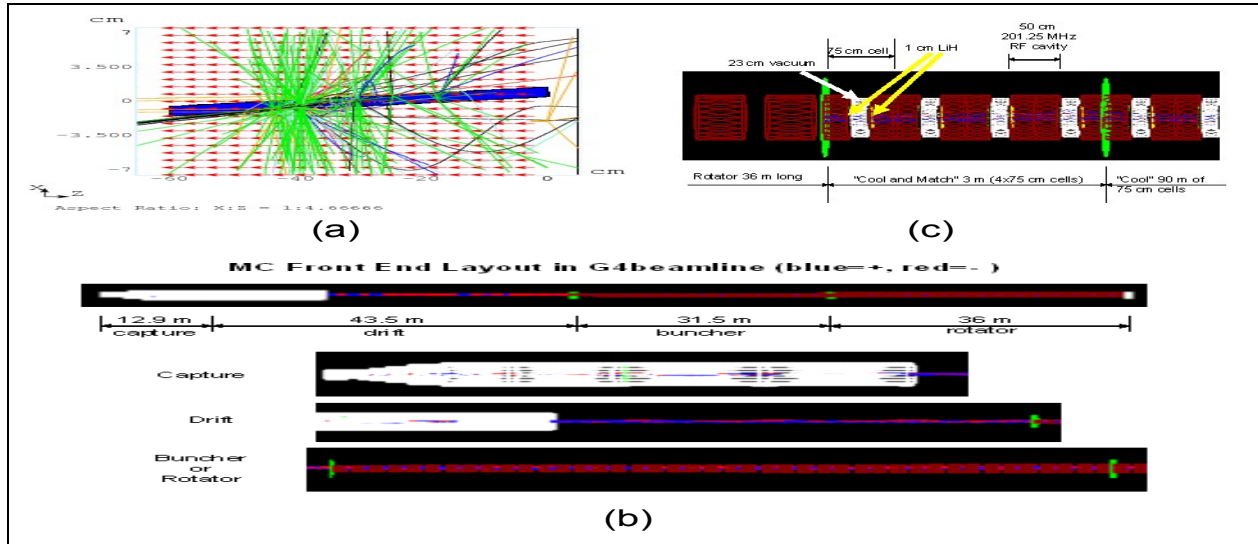


FIGURE 1. Layout of front end for neutrino factory or muon collider. (a) Protons (black line) of 8 GeV (kinetic energy) and 3 ns rms impinge on a Hg target with MARS-like [5] geometry. (b) The capture, drift, buncher, and rotator portions. (c) The “cool and match” and cool sections where “cool and match” refer to magnetic fields that transition from solenoidal field in rotator to alternating solenoids in cooler.

TABLE 1. High-level parameters of neutrino factory or muon collider front end layout.

$z(\text{m})$	Subsystem	Purpose	Physical Dimensions	Fields
-0.60 to 0.0	Targetry (MARS)	Produce copious amounts of pions	$L \approx 0.60 \text{ m}$ $R = 0.075 \text{ m}$	$B_{\text{sol}} = 20 \text{ T}$
0.0 to 12.9	Capture/Tapered Solenoid	Enhance pion/muon capture of both signs	$L = 12.9 \text{ m}$ $R = 0.075 \text{ m} \rightarrow 0.30 \text{ m}$	$B_{\text{sol}} = 20 \text{ T} \rightarrow 2 \text{ T}$
12.9 to 56.4	Drift	Develop momentum-time correlation	$L = 43.5 \text{ m}$ $R = 0.30 \text{ m}$	$B_{\text{sol}} = 2 \text{ T}$
56.4 to 87.9	Buncher	Adiabatically capture muons into RF buckets	$L = 31.5 \text{ m}$ $R = 0.30 \text{ m}$	$B_{\text{sol}} = 2 \text{ T}$ 42 RF Cavities: $E_{z,\text{max}} = 0 \rightarrow 15 \text{ MV/m}$ $f = 367 \text{ MHz} \rightarrow 238 \text{ MHz}$
87.9 to 123.9	Rotator	Energy-phase rotation	$L = 36 \text{ m}$ $R = 0.30 \text{ m}$	$B_{\text{sol}} = 2 \text{ T}$ 48 RF cavities $E_{z,\text{max}} = 15 \text{ MV/m}$ $f = 238 \text{ MHz} \rightarrow 202 \text{ MHz}$
123.9 to 126.9	Cool and Match	Transition from constant $B=2\text{T}$ in rotator to alternating solenoidal B in cooler.	$L = 3 \text{ m}$ $R = 0.30 \text{ m}$	$B_{\text{sol}} = 2 \text{ T} \rightarrow 2.3 \text{ T} \rightarrow -2.8 \text{ T}$ 4 RF cavities $E_{z,\text{max}} = 16 \text{ MV/m}$ $f = 201.25 \text{ MHz}$
126.9 to 216.9	Cool	Cool muon beam	$L = 90 \text{ m}$ $R = 0.30 \text{ m}$	$B_{\text{sol}} = -2.8 \text{ T} \leftrightarrow +2.8 \text{ T}$ 120 RF cavities $E_{z,\text{max}} = 16 \text{ MV/m}$ $f = 201.25 \text{ MHz}$

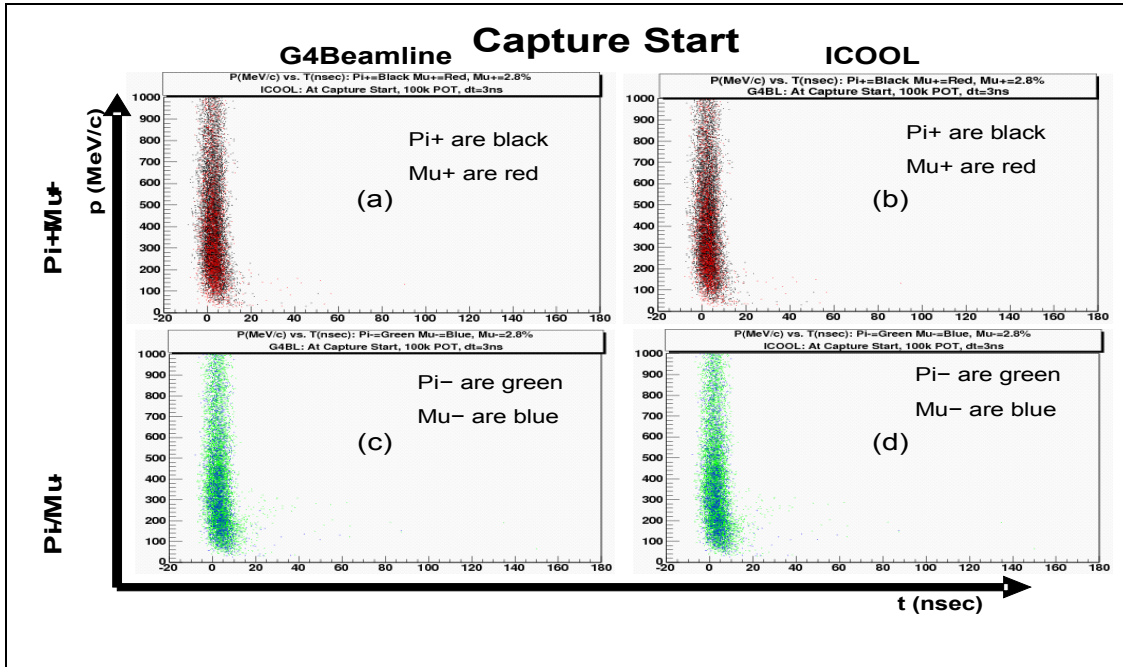


FIGURE 2. Momentum (MeV/c) vs. time (nsec) at start of capture solenoid (exit of production solenoid via MARS). Particle type that is more copious is plotted first with other type plotted on top. (a) π^+/μ^+ in G4beamline. (b) π^+/μ^+ in ICOOL. (c) π^-/μ^- in G4beamline. (d) π^-/μ^- in ICOOL.

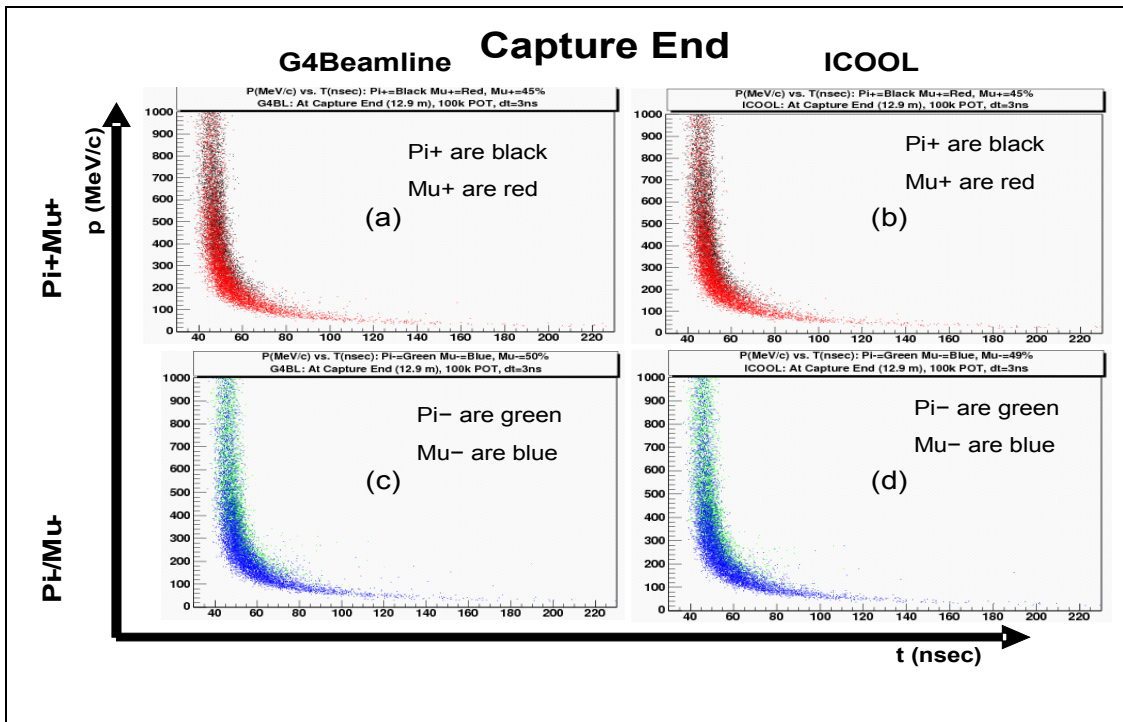


FIGURE 3: Momentum (MeV/c) vs. time (nsec) at end of capture. Particle type that is more copious is plotted first with other type plotted on top. (a) π^+/μ^+ in G4beamline. (b) π^+/μ^+ in ICOOL. (c) π^-/μ^- in G4beamline. (d) π^-/μ^- in ICOOL.

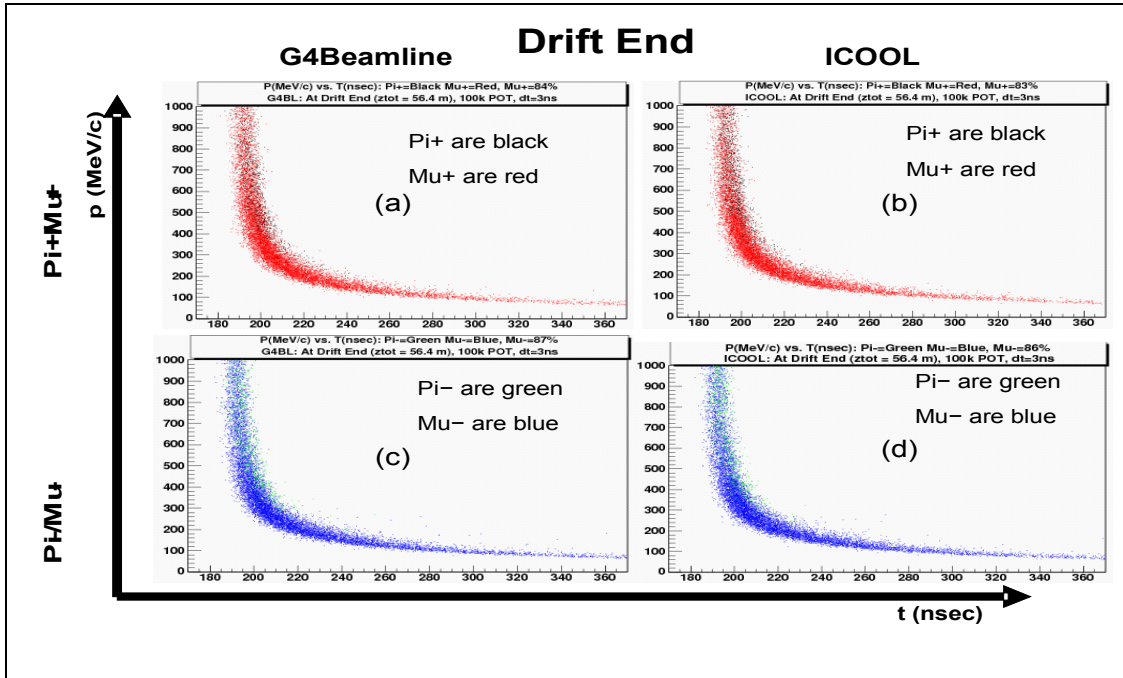


FIGURE 4: Momentum (MeV/c) vs. time (nsec) at end of drift. Particle type that is more copious is plotted first with other type plotted on top. (a) π^+/μ^+ in G4beamline. (b) π^+/μ^+ in ICOOL. (c) π^-/μ^- in G4beamline. (d) π^-/μ^- in ICOOL.

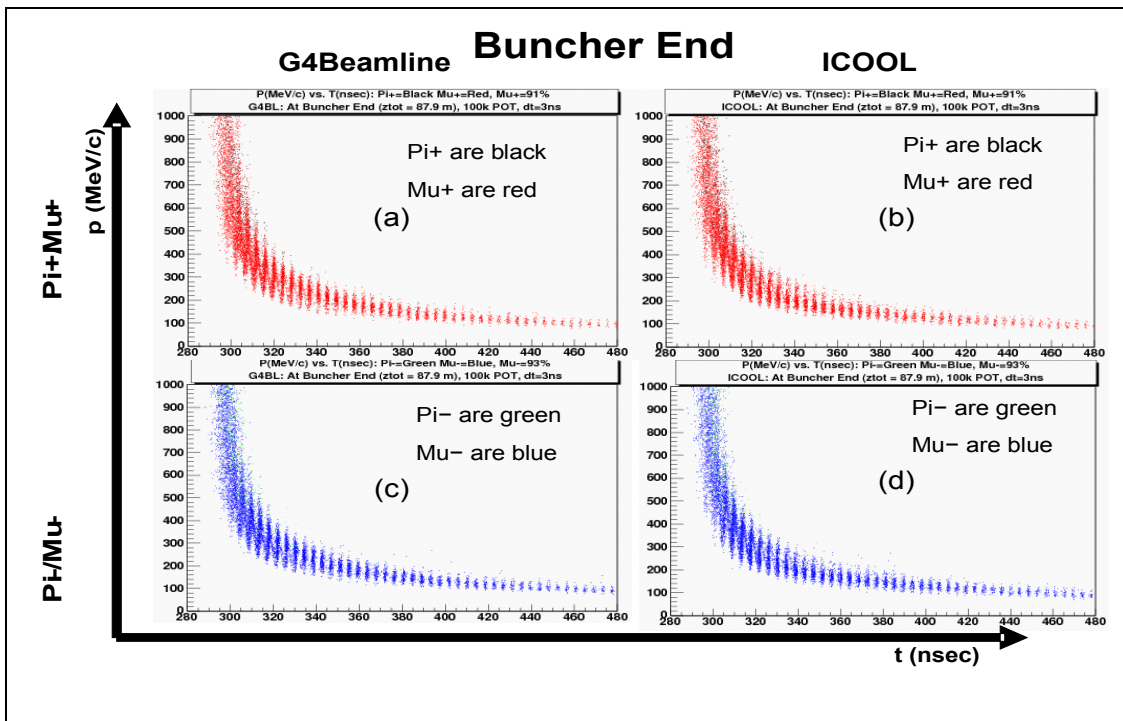


FIGURE 5: Momentum (MeV/c) vs. time (nsec) at end of buncher. Particle type that is more copious is plotted first with other type plotted on top. (a) π^+/μ^+ in G4beamline. (b) π^+/μ^+ in ICOOL. (c) π^-/μ^- in G4beamline. (d) π^-/μ^- in ICOOL.

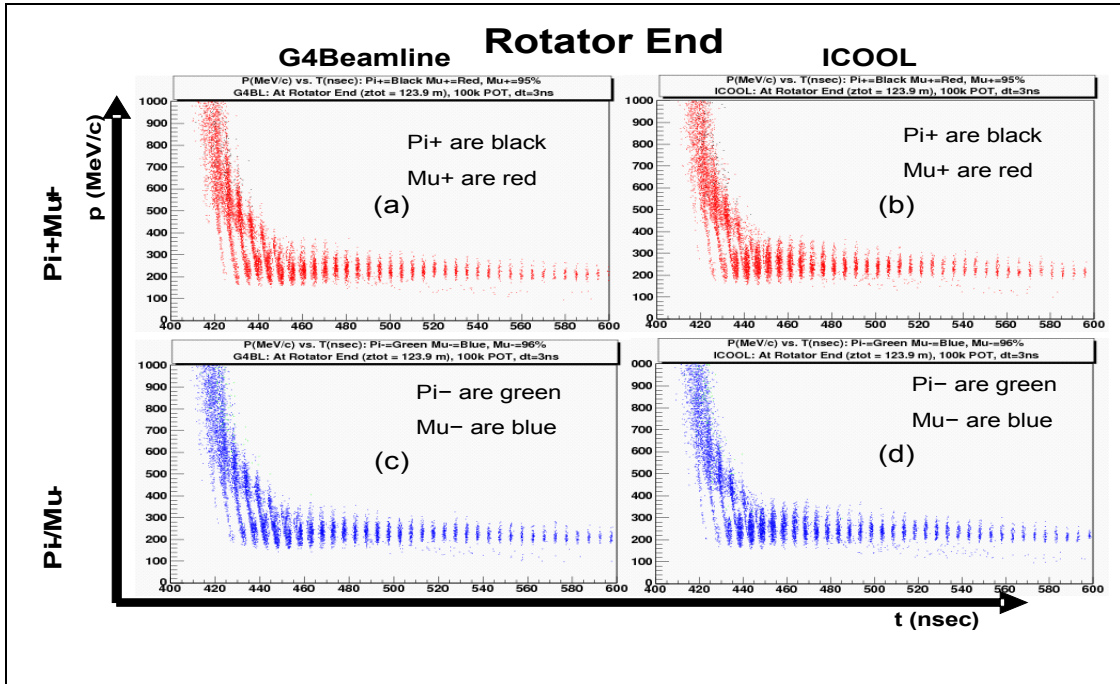


FIGURE 6: Momentum (MeV/c) vs. time (nsec) at end of rotator. Particle type that is more copious is plotted first with other type plotted on top. (a) π^+/μ^+ in G4beamline. (b) π^+/μ^+ in ICOOL. (c) π^-/μ^- in G4beamline. (d) π^-/μ^- in ICOOL.

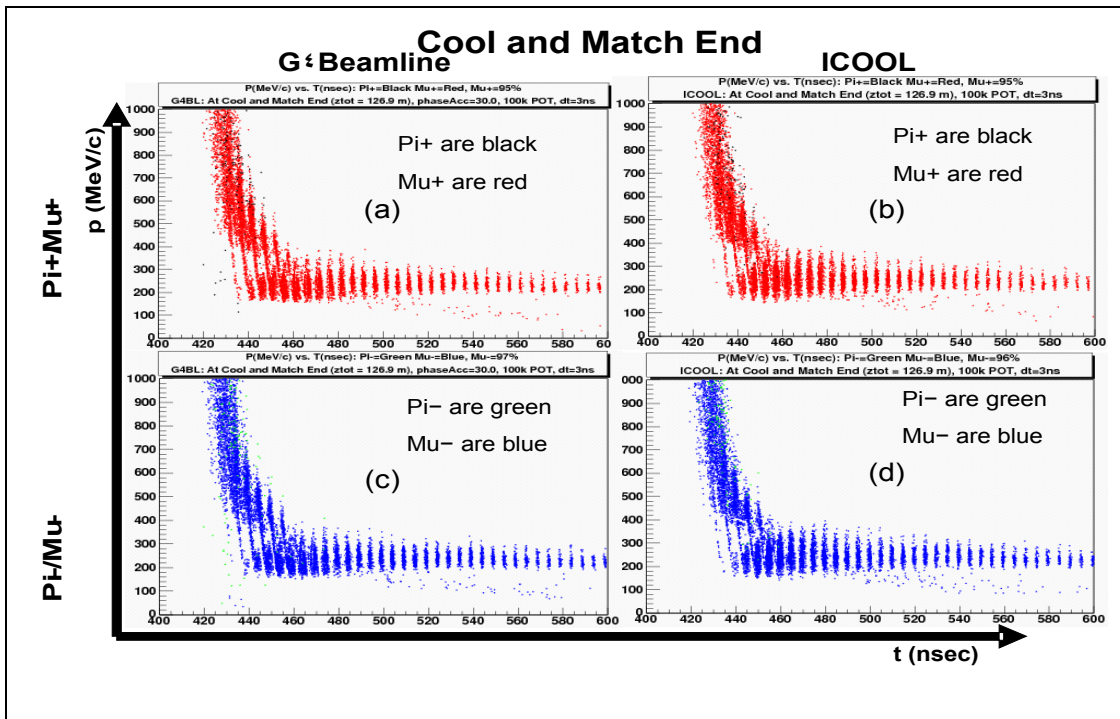


FIGURE 7: Momentum (MeV/c) vs. time (nsec) at end of cool and match section using default 30° phase for both ICOOL and G4beamline. Particle type that is more copious is plotted first with other type plotted on top. (a) π^+/μ^+ in G4beamline. (b) π^+/μ^+ in ICOOL. (c) π^-/μ^- in G4beamline. (d) π^-/μ^- in ICOOL.

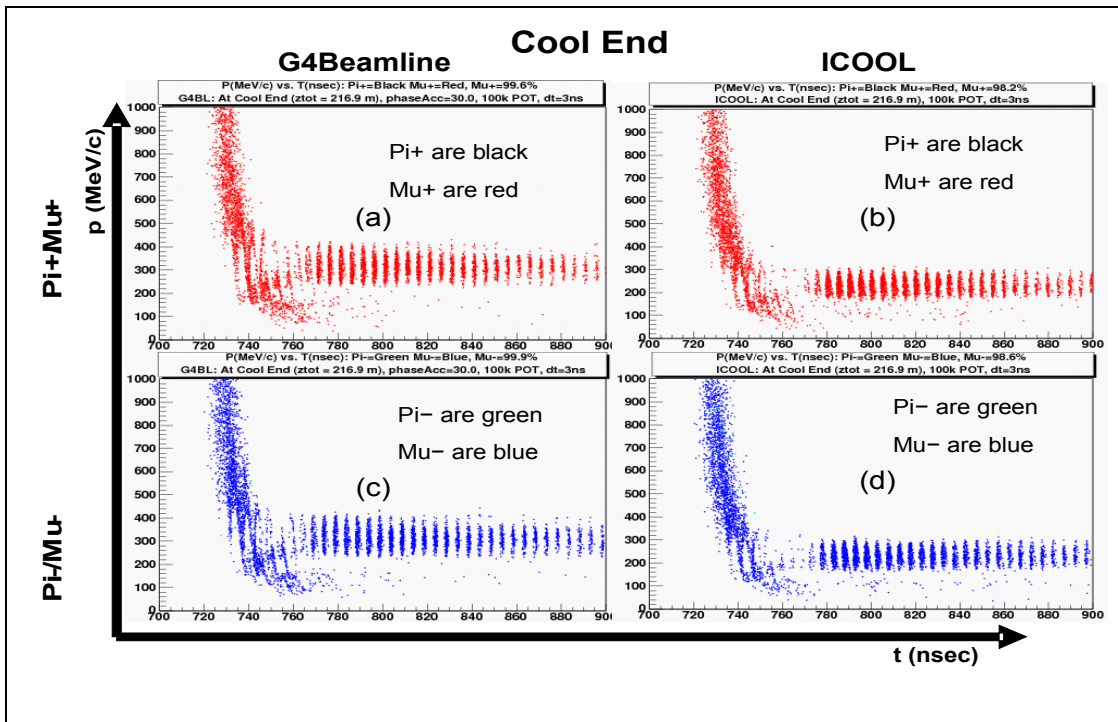


FIGURE 8: Momentum (MeV/c) vs. time (nsec) at end of cool section using default 30° phase for both ICOOL and G4beamline. Particle type that is more copious is plotted first with other type plotted on top. (a) π^+/μ^+ in G4beamline. (b) π^+/μ^+ in ICOOL. (c) π^-/μ^- in G4beamline. (d) π^-/μ^- in ICOOL.

Differences Between ICOOL and G4beamline in Cooling Portions and a Remedy

FIGURE 8 clearly shows differences between ICOOL and G4beamline at the end of the cooling channel. Muons at the end of the channel in G4beamline have higher average momenta and a wider momentum spread compared to its ICOOL counterpart. We consider the following possible sources to account for these differences:

1. Different rate of energy loss (dE/dx) for muons traversing LiH between ICOOL vs. G4beamline in “Cool and Match” and cool sections. Two remedies:
 - a. Adjust value of RF phase according to different energy loss.
 - b. Adjust density of material to provide same value of dE/dx and keep RF phase the same.
2. Different algorithm of RF phasing between ICOOL and G4beamline in volumes with material.

To study the differences between ICOOL and G4beamline in their characterization of the cooling material, LiH, μ^+ s were injected at the start of the cooling channel without RF nor magnetic fields for both simulators. The energy profile of the average muon energy is shown in FIGURE 9 to quantify this difference. The packing factor of LiH in the cooling section is $2\text{cm}/75\text{cm} = 0.02667$, so the resultant losses are $dE/dx|_{\text{ICOOL}} \approx 1.87 \text{ MeV/cm}$ and $dE/dx|_{\text{G4BL}} \approx 1.73 \text{ MeV/cm}$ for about an 8% lower energy loss in G4BL relative to ICOOL. If one were to scale this difference, the 30° RF phase in ICOOL would correspond to 27.4° in G4beamline, assuming that the 16 MV/m maximum gradient is maintained. However, instead of extrapolating the result (based on 7.5 m) over the lengthy 93 m channel, we instead decided to find an optimal phase in G4beamline that propagated muons from the start of the cooling channel with exactly $p=220 \text{ MeV/c}$ and maintained that momentum across the channel; FIGURE 10 shows that 25.8° is the best phase following this method. FIGURE 11 shows the momentum evolution of 500 μ^+ s, each starting with momentum of 220 MeV/c that propagate down the cooling channel using the optimal phase of 25.8° .

Another strategy to get around the difference between ICOOL and G4beamline is to modify a characteristic of LiH in one simulator to have its energy loss rate match the other. G4beamline allows an easy modification of the density and since dE/dx scales linearly with density, we chose to vary the density of LiH in G4beamline to have its $dE/dx|_{\text{G4BL}}$ match that of ICOOL, $dE/dx|_{\text{ICOOL}}$. FIGURE 12 shows energy loss of a muon with starting momentum of 220 MeV/c through the beginning of the cooling channel and that the density of 882.3 kg/m^3 for LiH in G4beamline produces a value for dE/dx that best matches that for ICOOL. FIGURE 13 shows acceptance and

emittances of ICOOL and G4beamline simulations down the cooling channel where G4beamline exercised two configurations: the default density for LiH using phase of 25.8° and the higher density LiH (to match ICOOL's dE/dx) using phase 30.0° . Neither of the G4beamline cases duplicates the ICOOL result, but the case with default density LiH using phase 25.8° exhibits a more monotonic acceptance along z that is also the case for ICOOL. Additionally, the entire strategy of increasing the density of LiH in G4beamline to match dE/dx of ICOOL has a problem in that the default density of LiH in G4beamline (820.0 kg/m^3) is already higher than that in ICOOL (780.0 kg/m^3). So, simply increasing the density in G4beamline for purpose of matching dE/dx in ICOOL enlarges this disparity. For all these reasons, we will not further consider increasing the density of LiH to rectify differences between G4beamline and ICOOL. Ultimately, we wish to understand the fundamental differences in the simulators with respect to how LiH is modeled, but we will defer this to a future study and simply continue to use a modified phase of 25.8° from ICOOL's 30.0° to account for the differences in dE/dx and for now assign this disparity as a systematic error due to uncertainty of how cooling is modeled in LiH.

Next, we investigate the effect of the different methods of RF phasing with respect to the reference particle. ICOOL sets the phasing of RF cavities with respect to the reference particle at constant velocity, ignoring slow down across material and speed up in RF cavities. G4beamline sets its phasing of RF cavities with respect to the reference, which does take into account the expected slow down in material and speed up in RF cavities. A direct comparison was performed within G4beamline to model both types of phasing to eliminate complications from other differences between ICOOL and G4beamline. The results in FIGURE 14 show effectively no effect due to the different phasing algorithms.

Finally, we show in FIGURE 15 the acceptance and emittance through the front end expected from both G4beamline (phase 25.8°) and ICOOL (phase 30.0°). There is a $\sim 16\%$ difference in the acceptance that grows in the cooling channel that is not currently understood, but is probably related to the larger amount of cooling provided in ICOOL (larger dE/dx in LiH and larger RF phase angle). This is currently under investigation. FIGURE 16 provides a measure of internal consistency where the equilibrium cooling momentum ($220 \text{ MeV}/c$) that is targeted in both G4beamline and ICOOL achieve similar momentum vs. time distributions for muons (and pions) at end of the cooling channel using phase of 25.8° in G4beamline and 30° in ICOOL. This is to be compared to FIGURE 8, which utilized 30.0° for both simulators.

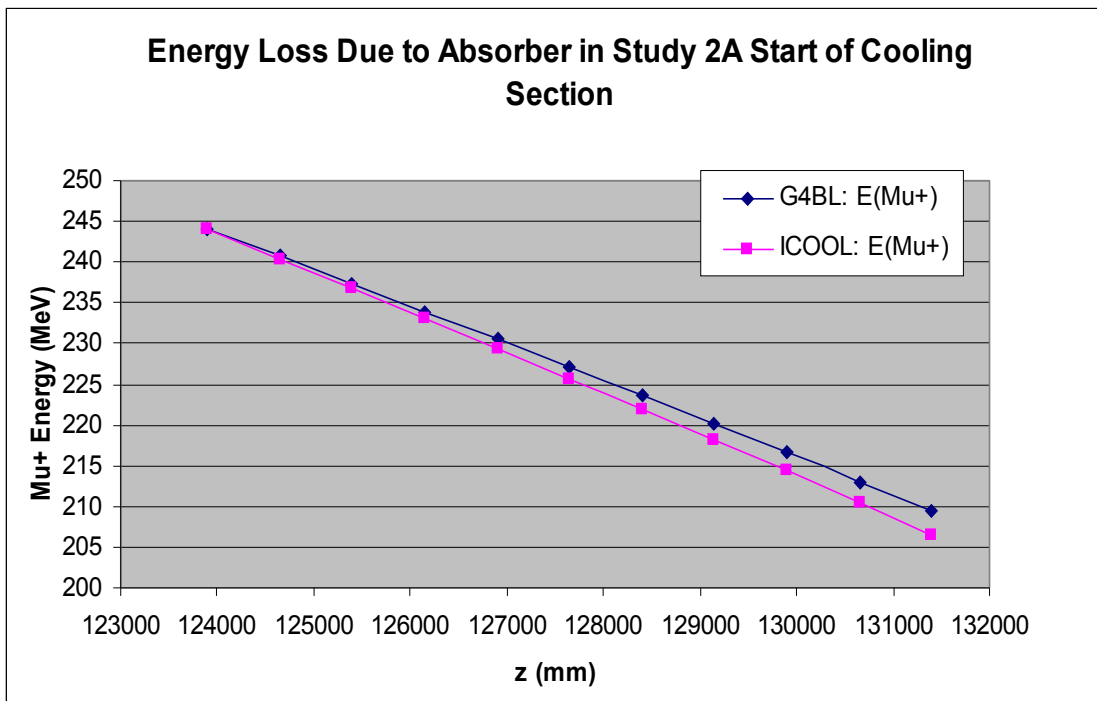


FIGURE 9: Energy loss in LiH for ICOOL and G4beamline. Packing factor of LiH is $2\text{cm}/75\text{cm} = 0.02667$. Resultant losses are $dE/dx|_{\text{ICOOL}} \approx 1.87 \text{ MeV/cm}$ and $dE/dx|_{\text{G4BL}} \approx 1.73 \text{ MeV/cm}$ for about 8% difference.

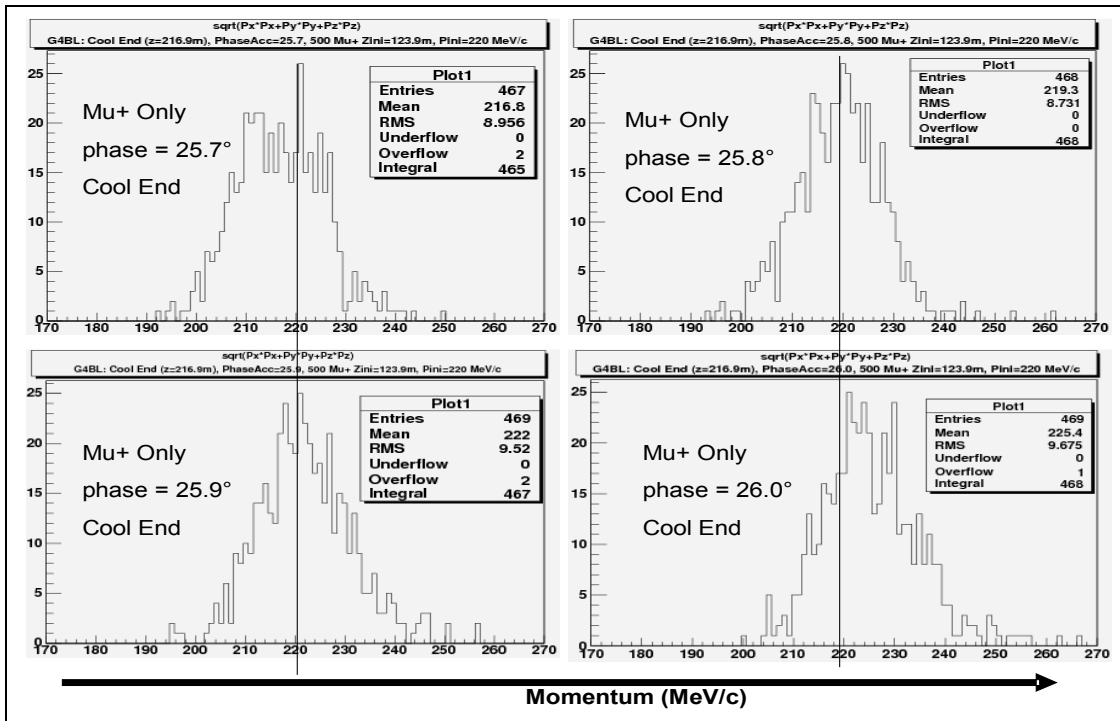


FIGURE 10: Determination of phase across cooling channel in G4beamline. Phase of 25.8° best maintains muon momentum of 220 MeV/c across the cooling channel.

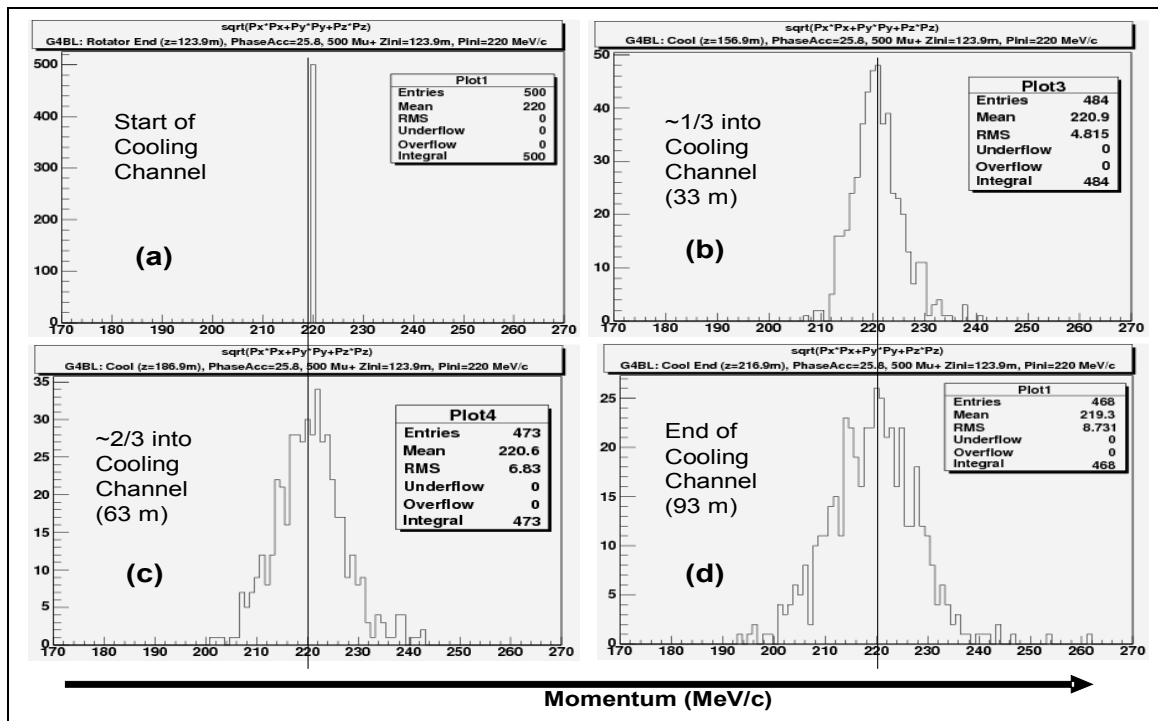


FIGURE 11: Momentum evolution of 500 μ^+ s with $p = 200$ MeV/c through cooling channel using optimal phase of 25.8°. (a) Muons produced with exactly 220 MeV/c at start of cooling section. (b) Momentum of muons at approximately 1/3 down cooling channel. (c) Momentum of muons at approximately 2/3 down cooling channel. (d) Momentum of muons at end of cooling channel.

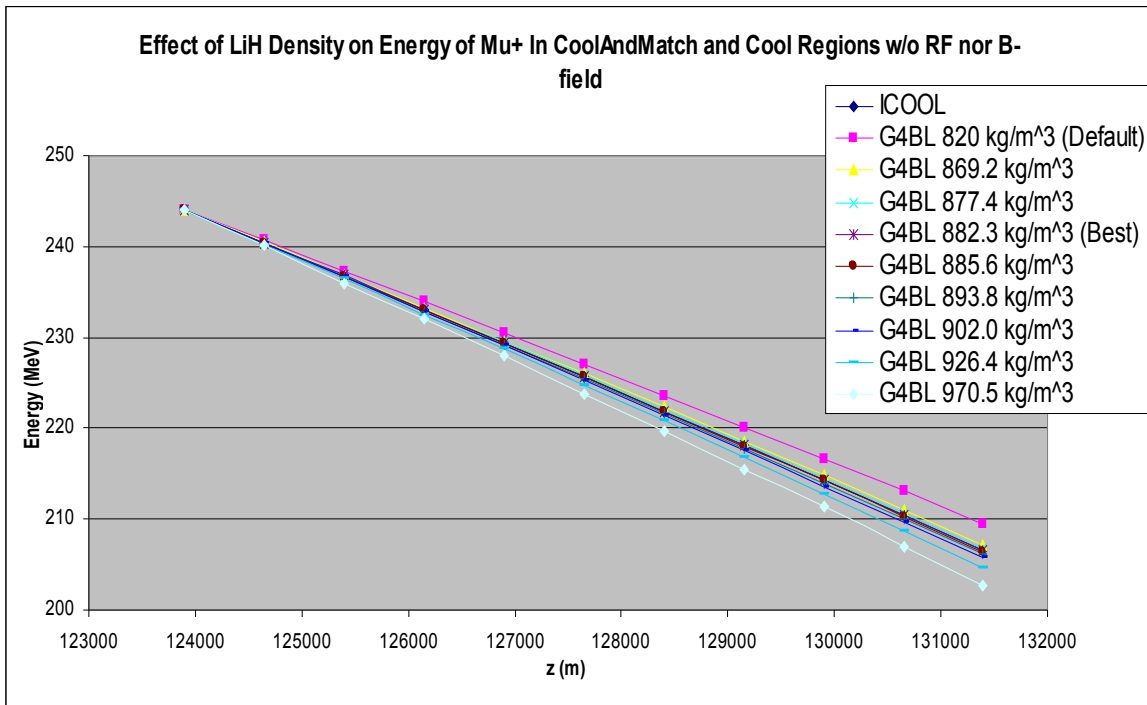


FIGURE 12: Effect of density of LiH on dE/dx in G4beamline. Density of 882.3 kg/m^3 provides $dE/dx|_{\text{G4BL}}$ that best matches $dE/dx|_{\text{ICOOL}}$.

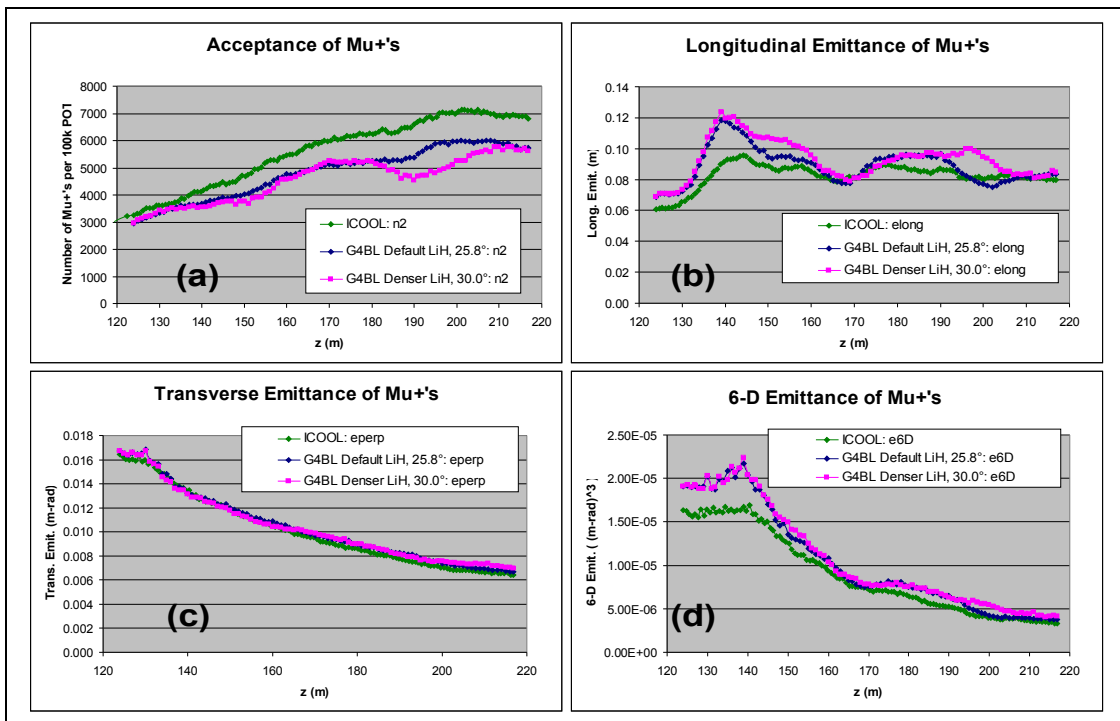


FIGURE 13: Effect of RF phase change vs. LiH density change in G4BL. Quantities are calculated using ECALC9. (a) Acceptance with cuts $A_{\text{trans}} < 0.030 \text{ m-rad}$, $A_{\text{long}} < 0.15 \text{ m-rad}$, and $n_e < 6.0$. (b) Longitudinal Emittance. (c) Transverse Emittance. (d) 6-D Emittance.

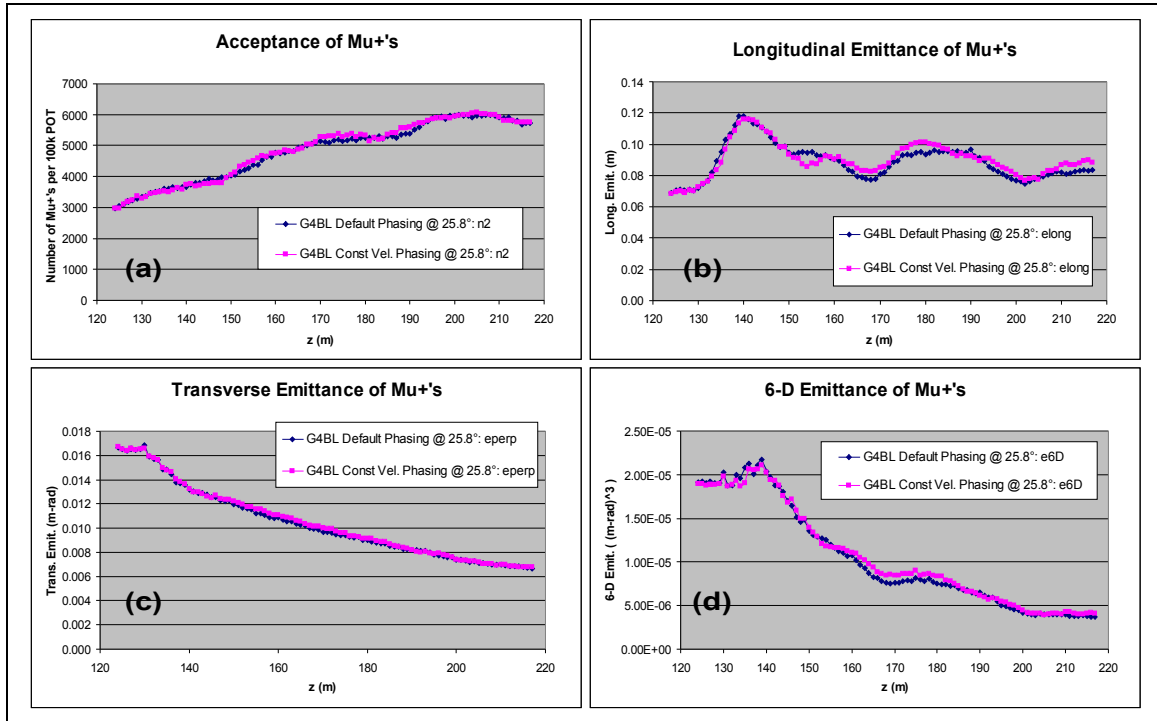


FIGURE 14: Effect of ICOOL phasing method (constant velocity) vs. G4beamline phasing method (deceleration in material; acceleration in RF). Study performed entirely in G4beamline to eliminate other systematic differences between ICOOL and G4beamline. Quantities are calculated using ECALC9. (a) Acceptance with cuts $A_{trans} < 0.030$ m-rad, $A_{long} < 0.15$ m-rad, and $n_e < 6.0$. (b) Longitudinal Emittance. (c) Transverse Emittance. (d) 6-D Emittance.

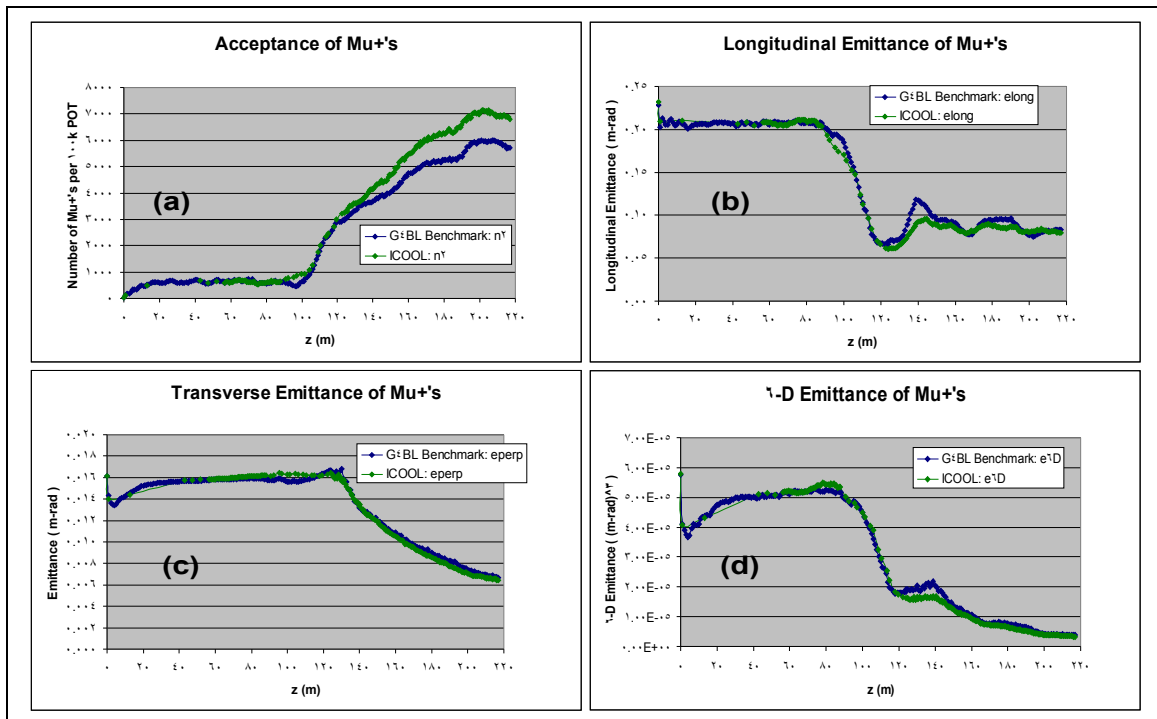


FIGURE 15: ICOOL vs. Benchmark G4beamline (G4BL) across front end. Benchmarked G4BL uses phase of 25.8° to account for differences in dE/dx in LiH (see FIGURE 9 and FIGURE 10). Quantities are calculated using ECALC9. (a) Acceptance with

cuts $A_{\text{trans}} < 0.030$ m-rad, $A_{\text{long}} < 0.15$ m-rad, and $n_{\sigma} < 6.0$. (b) Longitudinal Emittance. (c) Transverse Emittance. (d) 6-D Emittance.

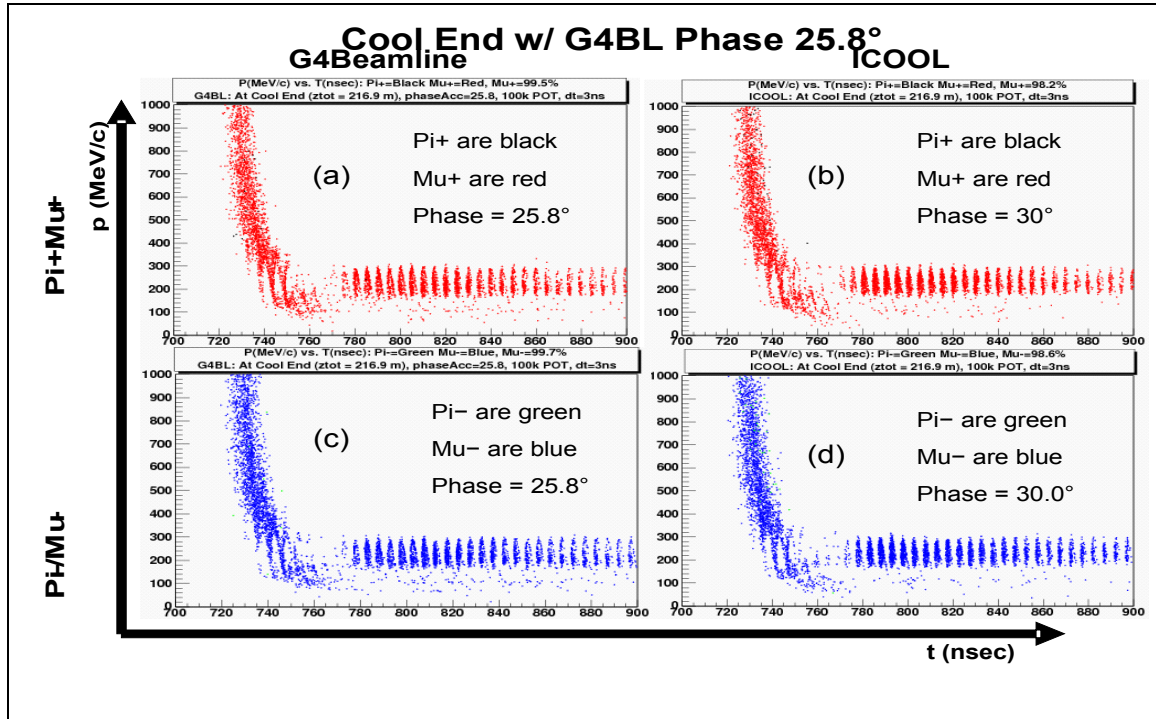


FIGURE 16: Momentum (MeV/c) vs. time (nsec) at end of cool section using phase of 25.8° in G4beamline (G4BL) and 30.0° for ICOOL. Particle type that is more copious is plotted first with other type plotted on top. (a) π^+/μ^+ in G4beamline. (b) π^+/μ^+ in ICOOL. (c) π^-/μ^- in G4beamline. (d) π^-/μ^- in ICOOL.

PRELIMINARY STUDY ON ECONOMIZING NUMBER OF RF CAVITIES

Another study was done to grasp the sensitivity of the buncher and rotator sections with respect to the granularity of frequencies and gradients used. The investigation was performed entirely in G4beamline, so complications from differences between G4BL and ICOOL are automatically avoided. The benchmark study allowed each RF cavity to implement its own ideal frequency based on two reference particles of different momenta being separated by a pre-selected number of RF wavelengths. In this particular case, we used 280 MeV/c and 154 MeV/c separated by 10 wavelengths in the buncher and 10.08 wavelengths in the rotator. Additionally, each RF cavity in the buncher had its maximum gradient rise according to:

$$G \text{ (MV/m)} = (6 \text{ MV/m}) (z / 31 \text{ m}) + (9 \text{ MV/m}) (z / 31 \text{ m})^2 \quad (1)$$

where z is the longitudinal location within the buncher. The maximum gradient in the rotator was 15 MV/m.

To test the sensitivity of the algorithm against the granularity of frequencies and field gradients, we grouped the cavities as follows:

1. Cavities in buncher and rotator were grouped into threes, where the set used a common frequency and gradient set by the middle cavity (Grp3RF)
2. Cavities in buncher and rotator were grouped into sixes, where the set used a common frequency and gradient set by average of the middle two cavities (Grp6RF)
3. Cavities in the buncher grouped into threes and cavities in the rotator grouped into sixes (Grp3&6RF) with frequencies and gradients set as in (1) and (2) above.
4. Cavities in the buncher grouped into sixes and cavities in the rotator grouped into threes (Grp6&3RF) with frequencies and gradients set as in (1) and (2) above.

Results for the acceptance and longitudinal emittance are shown in FIGURE 17, while transverse and 6-D emittances are in FIGURE 18. Differences in acceptance and emittances in the buncher and rotator sections appear

minimal until they are propagated through the cooling channel where differences in acceptance are magnified. If the cooling channel were to terminate at 200 meters (from start of capture tapered solenoid), we could realize cost savings associated with RF cavities using a common frequency and gradient in groups of three with only an expected ~5% reduction in acceptance.

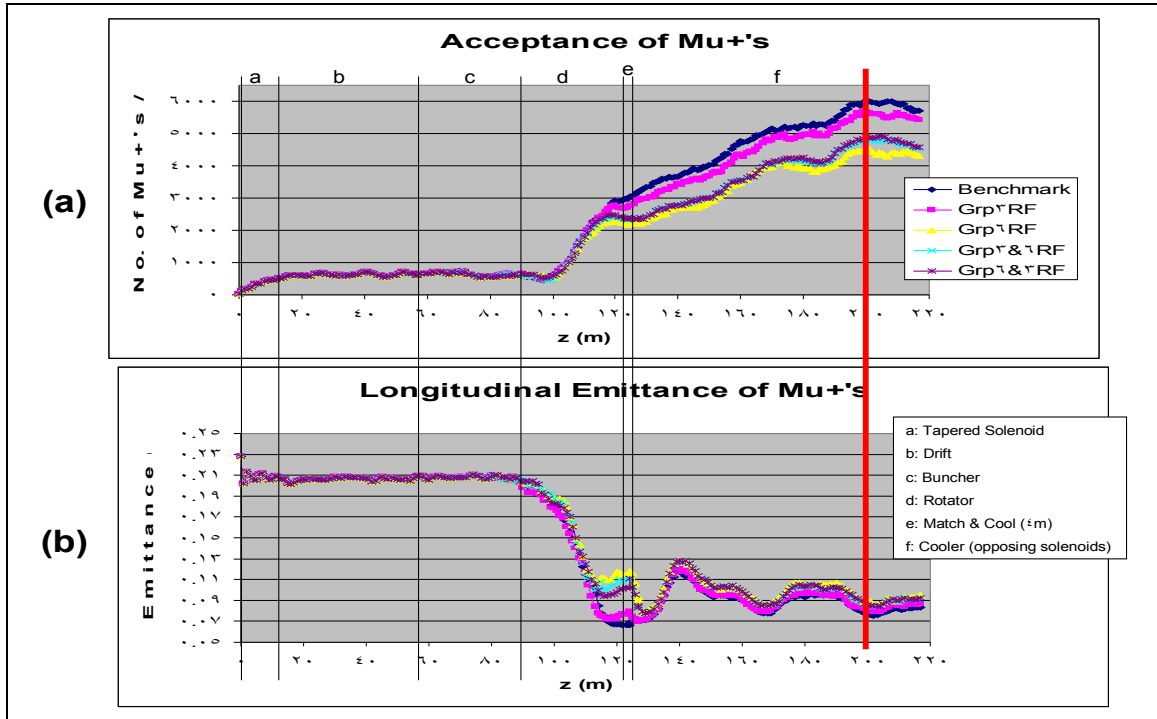


FIGURE 17: Economization of RF frequencies and gradients in buncher and rotator. Quantities are calculated using ECALC9. (a) Acceptance with cuts $A_{trans} < 0.030$ m-rad, $A_{long} < 0.15$ m-rad, and $n_{\sigma} < 6.0$. (b) Longitudinal emittance.

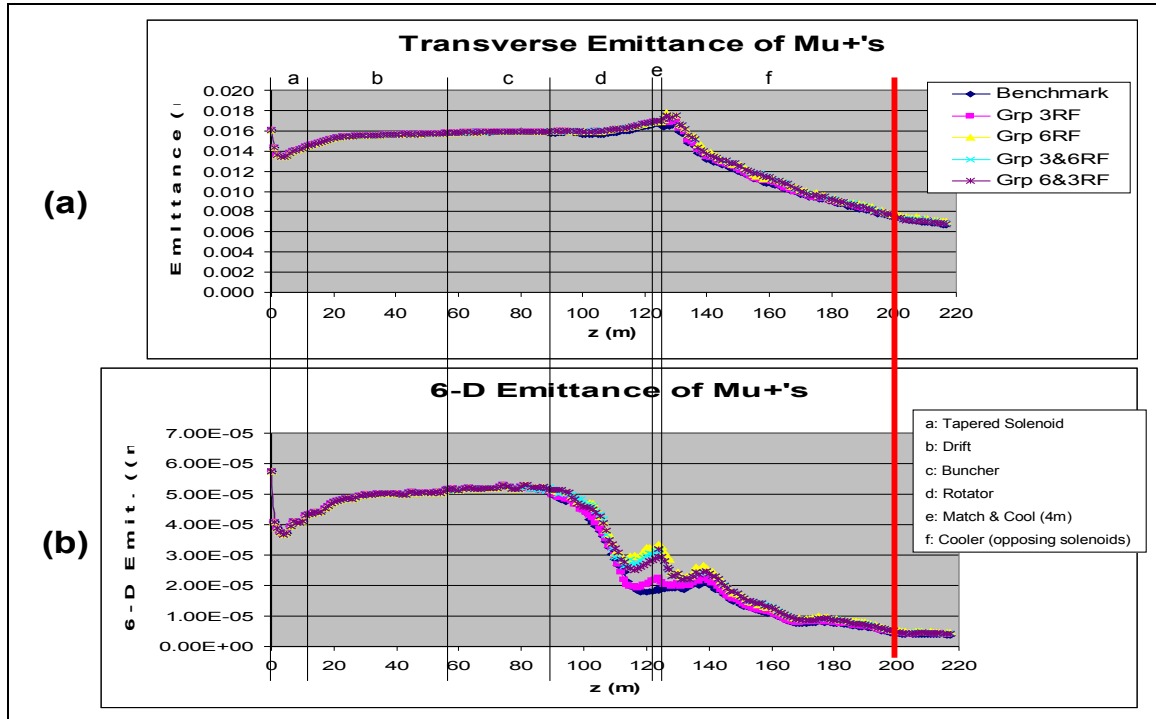


FIGURE 18: Economization of RF frequencies and gradients in buncher and rotator. Quantities are calculated using ECALC9. (a) Transverse emittance. (b) 6-D emittance

THOUGHTS ON EXTRACTING TOLERANCES FOR ENGINEERING REQUIREMENTS

Extracting tolerances for engineering requirements is straightforward. In some cases, modifications of a simulator are effectively required (timing of phase between RF cavities), while in others (alignment) it is a matter of convenience and speed as we will need to re-evaluate tolerances on future re-optimized designs. An example for RF phase timing would be a dump of the timing of each cavity for the reference particle, which serves as a basis for tolerance studies. External calculations are error prone and time consuming, as they generally would involve small studies of particles propagating across material, similar to that in FIGURE 9. A starting list of quantities that need to undergo tolerance evaluations are:

1. RF frequency
2. RF gradient
3. RF phase/timing
4. B-field strength and direction due to magnet itself
5. B-field strength and direction due to misalignment

It is imperative that these studies be performed on more than a single simulator for cross validation. Hence, we are dependent on enhancements of G4beamline and ICOOL to support these future studies.

CONCLUSION

We have performed an initial cross check of the baseline design for the front end of a muon collider and neutrino factory between ICOOL and G4beamline. We see consistency except in the cooling section, which is believed to be due to a difference in the modeling of the LiH cooling material. We will need to verify this and determine which simulator more accurately models reality.

Within G4beamline, we studied the different RF phasing algorithms. ICOOL uses constant velocity phasing, while G4beamline tracks the reference particle and phases according to slow down in material and speed up in RF cavities. We observed no differences due to these different RF phasing algorithms.

A preliminary study to economize number of RF frequencies and gradients was performed. This study also has relevance to tolerances expected of the system. The result is that we can reduce the number of frequencies and gradients by a factor of three at a price of reducing acceptance by about 5%.

Finally, in order to provide tolerances for a variety of engineering requirements on the current baseline design or any future re-optimized designs, enhancements to both G4beamline and ICOOL are required.

REFERENCES

1. Study 2A: <http://prst-ab.aps.org/abstract/PRSTAB/v9/i1/e011001>
2. ICOOL: <http://pubweb.bnl.gov/users/fernow/www/icool/>
3. G4beamline: <http://g4beamline.muonsinc.com>
4. GEANT4: <http://www.geant4.org/geant4/>
5. MARS: <http://www-ap.fnal.gov/MARS/>
6. MERIT: <http://cern.ch/merit/>